Occupant-Location-Catered Control of IoT-Enabled Building HVAC Systems

Amirkhosro Vosughi, Mengran Xue, and Sandip Roy

***Abstract*— This article studies about the catered controls for building heating-ventilation-air-conditioning (HVAC) systems, which react to the changing location of an occupant. A Markov jump-linear system model is developed which captures the building's thermal processes, HVAC system, occupant movement, and proposed proportional-integral-derivative feedback. A statistical analysis of the closed-loop dynamics is used to confirm moment boundedness and tune the control gains to improve temperature regularity with limited actuation, in the face of disturbances. The control strategy is demonstrated in an example.**

***Index Terms*— Home automation, heating-ventilation-air-conditioning (HVAC) systems, Markovian jump-linear systems (MJLSs), network control, stochastic Markov process.**

I. Introduction and Motivation

INTERNET-OF-THINGS (IoT) technologies are enabling new paradigms for thermal regulation of buildings [1]–[3], which exploit customized control of heating-ventilation-air-conditioning (HVAC) systems. One direction of particular interest is to design occupant-location-catered control schemes for temperature regulation. The main idea is to design HVAC controls to react to the occupants' current locations, to improve temperature regularization while possibly avoiding the excess energy use. Such controls can readily be deployed in new IoT-enabled buildings, e.g., using sensor networks and handheld mobile devices [4]–[7]. However, for these schemes to be effective, models and control designs are required that account for the building's thermal dynamics and weigh the benefits and drawbacks of reacting to the occupants' location profile.

In this article, occupant-location-catered building temperature regulation is studied, focusing on the base case with one occupant and a centralized HVAC system (or single control zone). The problem is phrased as a feedback-control task for a Markov jump-linear system (MJLS), which captures building heat flow in the presence of unmodeled disturbances, and the occupant's stochastic movement among the building's rooms. A proportional-integral (PI)-derivative (PID) controller is considered, which uses temperature measurements at the occupant's location to set the HVAC control input. A two-moment analysis of the closed-loop dynamics is developed and used to verify stochastic stability. Also, control-gain tuning is pursued, to shape a performance metric which combines the regularity of the occupied room's temperature and control effort.

The research described here connects to a wide literature on monitoring, control, and fault diagnosis of building thermal processes, using model-based approaches (see [8]–[17]). Recently, one focus in this literature has been to explore using new networking and IoT technologies to optimize HVAC systems, to improve control efficiency, support power-grid operations, or refine fault monitoring [18]. In a parallel track, monitoring and statistical analysis of occupant locations in buildings have been pursued, to support efficient operation [19]–[21]. An important recent effort on zone climate control in buildings has merged these tracks, by studying how occupancy information (whether measurements or predictions) can be used to save energy [20]. Relative to these studies, the main contribution of our work is to design controls for HVAC systems, which react to the changing location of a building occupant in real time. The proposed control scheme uses real-time sensing of temperatures and occupant locations, together with merged models for building thermal processes and occupant movement. The study demonstrates that catered controls of this type can be tuned for effective temperature regularization at the occupant's current location, while also requiring less actuation effort compare to control based on the thermostat in a fixed location.

Methodologically, this study draws on and contributes to the wide literature on MJLSs [22]–[26]. Specifically, our closed-loop analysis uses the two-moment analysis of MJLS. In addition, the special diffusive structure of the heat-flow dynamics is exploited to verify moment stability and obtain refined statistical characterizations for control tuning [25], [26].

Preliminary results in this direction were presented in [27]. In comparison, this study: 1) uses a detailed model for building thermal processes and HVAC operations; 2) captures disturbances; 3) generalizes the stability analysis to PID controllers; 4) includes proofs; and 5) further interprets gain tuning.

II. Modeling and Problem Formulation

Thermal processes in buildings are modeled at multiple resolutions. Here, an intermediate-resolution resistive capacitive (*RC*) network-type model is considered, which has previously been used for design of HVAC controls [8], [9], [14]–[16], [28]. The model represents a building as a network of walls and rooms (collectively, *nodes*), which act as thermal

Manuscript received May 3, 2018; revised November 26, 2018 and August 9, 2019; accepted August 14, 2019. Manuscript received in final form August 15, 2019. This work was supported by the United States National Science Foundation under Grant CNS-1545104 and Grant CMMI-1635184. Recommended by Associate Editor G. Hu. *(Corresponding author: Amirkhosro Vosughi.)*

The authors are with the School of Electrical Engineering and Computer Science, Washington State University, Pullman, WA 99164 USA (e-mail: amirkhosro.vosughi@wsu.edu; mxue@eecs.wsu.edu; sroy@eecs.wsu.edu).

Color versions of one or more of the figures in this article are available online at http://ieeexplore.ieee.org.

Digital Object Identifier 10.1109/TCST.2019.2936804

reservoirs [15]. It tracks nodal temperatures, which evolve through thermodynamic interactions deriving primarily from convection and conduction processes. Disturbances, including heat leakage to the outside, solar radiation, and indoor heat gains, are modeled as stochastic inputs.

Thermal regulation using a dual-duct variable air volume (VAV) HVAC system is modeled. In a VAV HVAC system, two constant-temperature air flows are used for heating and cooling the building [14], [16]. The air flow volume from each duct can be controlled, with only one duct being used at a time. The mass-transfer equations governing the dual-duct VAV are nonlinear. With the further assumption that the two air-flow temperatures are balanced around the desired temperature setpoint, the control can be modeled as a single two-way continuous-valued input and can be reasonably approximated as linear. Even when this assumption is relaxed, a single-input linear model is apt, so long as the setpoint temperature is sandwiched by the two air-flow temperatures [14].

Formally, a network with n nodes labeled $1, 2, \ldots, n$, is considered. The first r nodes $(1, \ldots, r)$ represent rooms, while the remaining nodes represent w_1 exterior walls (nodes $r+1, \ldots, r+w_1$) and w_2 interior walls (nodes $r+w_1+1, \ldots, r+w_1+w_2=n$). The temperature $x_i(t)$ of each node i is tracked in continuous time. For the VAV HVAC system, the node (room and wall) temperatures $x_i(t)$ can be modeled as follows [14]:

$$\dot{x}_i(t) = \frac{1}{m_i}\left(\sum_{j=1}^{n} w_{ij}(x_j - x_i) - w_{io}x_i + \gamma_i \rho V c_p (T_0 - x_i) + d_i(t)\right) \tag{1}$$

where $m_i > 0$ is the thermal capacitance of node i, $w_{ij} = w_{ji}$ is the thermal conductance between nodes i and j, w_{io} is the equivalent thermal conductance to the outside of node i, V is the volume flow rate from the HVAC system (which is the control input), T_0 is the constant temperature of the HVAC air flow, ρ is the density of the air, c_p is the specific heat capacity of the air, γ_i specifies the fractions of the HVAC air volume that flow to each node (where $\gamma_i \geq 0$ for $i = 1, \ldots, n$ and $\gamma_i = 0$ for other i), and $d_i(t)$ indicates the disturbance at node i. In addition, the thermal conductances w_{ij} and w_{io} are greater than zero only if there is a direct thermal link between the nodes (or to the outside), and are zero otherwise.

The following disturbances $d_i(t)$ are considered. The rooms (nodes $i \in \{1, \ldots, r\}$) are modeled as being subjected to unmeasured heat gains. Exterior walls (nodes $i \in \{r+1, \ldots, r+w_1\}$ are subject to solar radiation and heat flow due to the outside temperature. The total disturbance input for the exterior walls can be expressed in more detail as $d_i(t) = \alpha q''_{rad_i} a_i + T_\infty w_{io}$ where q''_{rad_i} is total radiative energy that impinges on the exterior wall i per unit area, α is absorptivity of surface, a_i is area of exterior wall i exposed to sun, $w_{oi} = w_{io}$ is the thermal conductance between exterior wall i and the outside, and T_∞ is the outside temperature. We stress that the heat flows into the building due to the external temperature is modeled as a disturbance; this thermal flow is sometimes alternately represented directly in the second term on the right side of (1), as a temperature differential. For the remaining nodes (interior walls), we assume that the disturbances are minimal ($d_i(t) = 0$), however, the analysis allows for the representation of disturbances if desired. Broadly, the disturbances impacting the building thermal dynamics can be modeled as stochastic processes with slowly varying parameters, summed with gradually varying deterministic signals. For our analysis, we represent the disturbance over the time horizon of interest as a stationary two-moment-bounded stochastic process but include time-varying disturbances in simulations.

Remark 1: Several simplifications in our formulation should be noted. We have not modeled time-varying mass flows between rooms, which could be captured as stochastic variations in the conductance. Although such variations are not considered in our formal analyses, they can be captured in simulations. In addition, we have ignored variations in temperatures within nodes, assumed a constant specific heat for the air, and excluded latent loads.

Remark 2: More detailed formulations of the building HVAC model present separate equations for the thermal dynamics of rooms and walls [29]. These formulations are instructive for understanding parameterization and model identification but are omitted here to save space.

Equation (1) is nonlinear, since the heat input from the HVAC system in (1) involves a product of a control and state variable (the volume flow rate and temperature). The model can be linearized around the equilibrium point at which the room temperatures equal a typical setpoint, see [14] for details. The linearized dynamics can be expressed in a matrix form as $\dot{\mathbf{x}} = A\mathbf{x}(t) + Bu(t) + D(t)$, where $\mathbf{x} = [x_1 \ \cdots \ x_{n-1} \ x_n]^{\mathbf{T}}$. The matrix A is an $n \times n$ matrix where $A_{ij} = (w_{ij}/m_i)$ for $i = 1, \ldots, n$, $j = 1, \ldots, n$, $j \neq i$; and the diagonal elements A_{ii}, $i = 1, \ldots, n$ are given by $A_{ii} = -\sum_{j \neq i}(w_{ij}/m_i) - (w_{io}/m_i)$. The input matrix B is an $n \times 1$ matrix with entries $B_i = \gamma_i(c_p/m_i)(T_0 - \overline{y}_{\text{ref}})$ for $i \in \{1, \ldots, r\}$, and the remainder of the entries equal to zero, $\overline{y}_{\text{ref}}$ is the setpoint temperature around which the linearization has been done, the input $u(t)$ is the volume flow rate out of the HVAC system (V). Also, $D(t)$ is the disturbance vector with n entries, whose ith element is equal to $(d_i(t)/m_i)$.

The movement of a single occupant among the building's rooms is considered. The occupant's room location is modeled as a Markov process. Several models for the building-occupant mobility have been developed, primarily in the indoor sensor networking literature [30]. Markov-chain models for occupant locations are also consistent with Markov models for occupancy counts in rooms. While a Markov representation is approximate, it is apt for the statistical analysis of HVAC control considered here. The HVAC controller is assumed to be alerted to the occupant's location (room) at the times $t = kT$ for $k = 0, 1, 2, \ldots$, where T is a sampling period. Furthermore, accurate temperature measurements at the occupant's current location are available to the HVAC controller at these times (with minimal delay). A finite-state Markov chain can be used to model the room location $s[k]$ at the data-transmission times $t = kT$. Note that $s[k]$ may take on values among $1, \ldots, r$, corresponding to the r rooms. The $r \times r$ transition matrix for the room-location Markov chain is denoted by $P = \left[p_{ij}\right]$, and is assumed to be ergodic.

Also, we define the temperature observation $y[k]$ as the temperature of the occupied room sampled at time $t = kT$, i.e., $y[k] = x_{s[k]}(kT)$. For our analysis, it is more convenient to express the observed temperature as a time-varying projection of the state $\mathbf{x}(t)$. Specifically, we have that $y[k] = \overrightarrow{v}^T[k]\mathbf{x}(kT)$, where $\overrightarrow{v}^T[k] = [\overrightarrow{e}^T[k]\ \overrightarrow{0}^T]$, where $\mathbf{e}[k]$ is a 0–1 indicator vector for the occupant's room location $s[k]$ and $\overrightarrow{0}$ is zero row vector with length $w_1 + w_2$. The occupant location chain is assumed to be independent of the disturbance.

The HVAC controller aims to regulate the temperature at the occupant's current location (room) at a desired reference temperature y_{ref}, by adjusting the air flow input $u(t)$. Here, a PID control scheme is considered, based on the need for portable, robust, and easy-to-implement solutions. Data transmission and computation for networked control schemes are typically clocked, and data rates for building controls are sufficiently fast compared to the thermal dynamics of the building. With this in mind, it is natural to apply a zero-order-hold control, for which the control input is updated after each data transmission and held constant in between. The following PID control scheme of this form is proposed: $u(t) = u[k]$ for $kT \le t < (k+1)T$, where $u[k] = K_p(y_{\text{ref}} - y[k]) - K_d(y[k] - y[k-1])/T + K_i \sum_0^k (y_{\text{ref}} - y[k]) \times T$, and where K_p, K_d and K_i are proportional, derivative, and integral gains.

Remark 3: Multiple occupants can be represented using an expanded Markov chain that tracks occupant-location configurations. Likewise, multiple zone controllers can be represented with a multi-input plant model. These generalizations admit the same statistical analyses as the model considered here; however, the controller design becomes more sophisticated, and computation also increases.

III. Controller Analysis and Design

The main focus of this work is to: 1) develop a statistical analysis of the closed-loop dynamics of the HVAC system in the face of disturbances and 2) pursue tuning of the control gains to shape a combined temperature-regularity- and actuation-effort-based performance metric. To enable this analysis, the closed-loop state dynamics are reformulated as a discrete-time MJLS (Section III-A). Then, a two-moment statistical analysis is undertaken by drawing on standard machinery for MJLS (Section III-B). Then stability (statistical boundedness of the temperature deviation) is confirmed, using an eigenanalysis of the moment recursion (Section III-C). Finally, the quadratic performance metric is characterized, and gain tuning to shape the metric is pursued (Section III-D).

A. Reformulation as an MJLS

The linearized closed-loop dynamics at the data-transmission times are reformulated as a discrete-time MJLS. This reformulation requires defining an extended state vector $\overrightarrow{\xi}$ with $l = n + r + 1$ entries, as

$$\overrightarrow{\xi}[k] = \begin{bmatrix} \overrightarrow{\theta}[k] \\ \overrightarrow{\kappa}[k-1] \\ Acc[k] \end{bmatrix}$$

where $\overrightarrow{\theta}[k] = \mathbf{x}[k] - y_{\text{ref}}\overrightarrow{1}$ is a temperature tracking error vector from to the reference (goal) temperature, $\overrightarrow{1}$ is a vector with all unity entries, $\kappa[k]$ is the first r entries of $\theta[k]$, $Acc[k] = \sum_{m=1}^{k} z[m]$ is an accumulator for the integral controller, and $z[m] = \overrightarrow{v}^T[m]\overrightarrow{\theta}[m]$ indicates the temperature of the occupied room in the shifted coordinates.

The extended state vector $\overrightarrow{\xi}[k]$ is governed by a discrete-time Markovian jump linear process, which can be obtained by solving the continuous-time dynamics over intervals of duration T for each underlying occupant-location state

$$\overrightarrow{\xi}[k+1] = G_c^{\text{PID}}(i)\overrightarrow{\xi}[k] + \bar{D}[k] \tag{2}$$

where the $l \times l$ matrix $G_c^{\text{PID}}(i)$ is a function of the underlying Markov chain state i (the room where the occupant is located), and $\bar{D}[k] = \begin{bmatrix} D[k] \\ \overrightarrow{0} \end{bmatrix}$ where $D[k]$ is an n-element vector. The matrices $G_c^{\text{PID}}(i)$, $i = 1, \ldots, r$, and $D[k]$ can be calculated as

$$G_c^{\text{PID}}(i) = G_A^{\text{PID}}(i) + G_p^{\text{PID}}(i) + G_d^{\text{PID}}(i) + G_i^{\text{PID}}(i) \tag{3}$$

$$D[k] = \int_0^T e^{A\tau} D(kT + \tau) d\tau \tag{4}$$

where

$$G_A^{\text{PID}}(i) = \begin{bmatrix} \bar{A} & 0_{n\times r} & 0_{n\times 1} \\ I_{r\times n} & 0_{r\times r} & 0_{r\times 1} \\ v^T(i) & 0_{1\times r} & 1 \end{bmatrix}$$

$$G_p^{\text{PID}}(i) = -K_p \Phi_{\bar{\beta}} \begin{bmatrix} S_2(i) & 0_{n\times r} & 0_{n\times 1} \\ 0_{r\times n} & 0_{r\times r} & 0_{r\times 1} \\ 0_{1\times n} & 0_{1\times r} & 0 \end{bmatrix}$$

$$G_d^{\text{PID}}(i) = \frac{-K_d}{T} \Phi_{\bar{\beta}} \begin{bmatrix} S_2(i) & -S_3(i) & 0_{n\times 1} \\ 0_{r\times n} & 0_{r\times r} & 0_{r\times 1} \\ 0_{1\times n} & 0_{1\times r} & 0 \end{bmatrix}, \text{ and}$$

$$G_i^{\text{PID}}(i) = -K_i T \Phi_{\bar{\beta}} \begin{bmatrix} S_2(i) & 0_{n\times r} & 1_{n\times 1} \\ 0_{r\times n} & 0_{r\times r} & 0_{r\times 1} \\ 0_{1\times n} & 0_{1\times r} & 0 \end{bmatrix}.$$

Here, $\bar{A} = e^{AT}$ and $\Phi_{\bar{\beta}}$ is $l \times l$ diagonal matrix whose jth diagonal element is equal to jth entry of the vector $\Phi_\beta = \Phi B$ for $j = 1, \ldots, n$ and is equal to zero otherwise, $\Phi = \int_0^T e^{A(\tau)} d\tau$, and S_2 is an $n \times n$ matrix whose ith column is a unity vector while all other entries are 0. Similarly, S_3 is $n \times r$ matrix that ith column is a unity vector while all other entries are 0 and $I_{r\times n} = [I_{r\times r}, 0_{r\times(n-r)}]$. Note that the matrix $G_A^{\text{PID}}(i)$ in the above expression describes the internal heat-exchange dynamics and the evolution of the accumulator state $Acc[k]$, while $G_p^{\text{PID}}(i)$, $G_d^{\text{PID}}(i)$, and $G_i^{\text{PID}}(i)$ describe the effects of the proportional, derivative, and integral control terms, respectively. We note also that $D[k]$ is stationary and two-moment bounded.

B. Two-Moment Analysis

The reformulation developed above allows the application of the standard machinery for MJLS, see [22]–[24]. First, the analysis of state moments for MJLS can be directly applied to the closed-loop model [22]–[24]. In particular, a two-moment analysis can be developed by considering the Kronecker product vectors $\psi_1[k] = \overrightarrow{v}^T[k] \otimes \xi[k]$ and

$\psi_2[k] = \overrightarrow{v}^T[k] \otimes \xi[k]^{\otimes 2}$, which contain products of the extended state vector entries with an indicator of the underlying Markov chain's status and the notation $(Q)^{\otimes 2}$ refers to the self-Kronecker product of the matrix Q. The vectors $\psi_1[k]$ and $\psi_2[k]$ have lengths lr and l^2r, respectively. Per the standard analysis of MJLS [22]–[24], the *first-moment vector* $E(\psi_1[k])$ and the *second-moment vector* $E(\psi_2[k])$ are governed by the following linear time-invariant dynamics or recursions: $E(\psi_1[k+1]) = H_1^{\text{PID}} E(\psi_1[k]) + \tilde{D}_1[k]$, where

$$H_1^{\text{PID}} = \begin{bmatrix} p_{11}G_c^{\text{PID}}(1) & \cdots & p_{1r}G_c^{\text{PID}}(r) \\ \vdots & \ddots & \vdots \\ p_{r1}G_c^{\text{PID}}(1) & \cdots & p_{rr}G_c^{\text{PID}}(r) \end{bmatrix}$$

r is the number of states in the underlying Markov chain (the number of indoor rooms). Also, $\tilde{D}_1[k] = \bar{P}_l D_1[k]$ where

$$D_1[k] = \begin{bmatrix} E(\bar{D}[k])P(s[k]=1) \\ \vdots \\ E(\bar{D}[k])P(s[k]=r) \end{bmatrix}.$$

$\bar{P}_l = P \otimes I_l$, I_l is an identity matrix of dimension l, $E(\bar{D}[k]|s[k]=j)$ is the expectation of the disturbance vector, $P(s[k]=j)$ is the observer's location probability, and we have used the independence of the disturbance signal and the occupant's location.

Likewise, we have that $E(\psi_2[k+1]) = H_2^{\text{PID}} E(\psi_2[k]) + H_{12} E(\psi_1[k]) + \tilde{D}_2[k]$,
where

$$H_2^{\text{PID}} = \begin{bmatrix} p_{11}G_c^{\text{PID}}(1)^{\otimes 2} & \cdots & p_{1r}G_c^{\text{PID}}(r)^{\otimes 2} \\ \vdots & \ddots & \vdots \\ p_{r1}G_c^{\text{PID}}(1)^{\otimes 2} & \cdots & p_{rr}G_c^{\text{PID}}(r)^{\otimes 2} \end{bmatrix} \text{ and}$$

$$H_{12}^{\text{PID}} = \begin{bmatrix} p_{11}G_D^{\text{PID}}(1) & \cdots & p_{1r}G_D^{\text{PID}}(r) \\ \vdots & \ddots & \vdots \\ p_{r1}G_D^{\text{PID}}(1) & \cdots & p_{rr}G_D^{\text{PID}}(r) \end{bmatrix}$$

$$\tilde{D}_2[k] = \bar{P}_{l^2} D_2[k]$$

$$D_2[k] = \begin{bmatrix} E(\bar{D}[k]^{\otimes 2})P(s[k]=1) \\ \vdots \\ E(\bar{D}[k]^{\otimes 2})P(s[k]=r) \end{bmatrix}.$$

Also, $G_D^{\text{PID}}(i) = G_c^{\text{PID}}(i) \otimes E(\bar{D}[k]) + E(\bar{D}[k]) \otimes G_c^{\text{PID}}(i)$, $\bar{P}_{l^2} = P \otimes I_{l^2}$ and I_{l^2} is the identity matrix with dimension l^2. Note that the independence of the disturbance from the occupant location has again been exploited. Also, from the fact that the disturbance is assumed to be mean-stationary, the matrices $G_D^{\text{PID}}(i)$ are seen to be fixed rather than time-varying.

The entries in the first- and second-moment vectors identify the conditional moments of the extended state vector. For example, the first moment vector can be written as

$$E(\psi_1[k]) = \begin{bmatrix} E(\xi[k]|s[k]=1)P(s[k]=1) \\ \vdots \\ E(\xi[k]|s[k]=r)P(s[k]=r) \end{bmatrix} \quad (5)$$

where $E(\xi[k]|s[k]=j)$ is the conditional expectation of the extended state given the observer's location. Also

$$E(\psi_2[k]) = \begin{bmatrix} E(\xi[k]^{\otimes 2}|s[k]=1)P(s[k]=1) \\ \vdots \\ E(\xi[k]^{\otimes 2}|s[k]=r)P(s[k]=r) \end{bmatrix}. \quad (6)$$

Thus, the first two moments of the temperature in the occupant's current room as well as of the input can be directly computed from the first- and second-moment vectors, at either the data-transmission times or at intermediate times. In this way, the deviation of the occupied room's temperature from the desired value and control effort can be statistically characterized, for the closed-loop system.

C. Stability Analysis

Evaluation and design of the occupant-location-catered control require characterization of the closed-loop performance. As a first step, closed-loop stability in the sense of asymptotic moment boundedness is verified. One would expect a low-gain control scheme to achieve moment boundedness, since the open-loop process is strictly stable. However, the stability analysis has some subtlety because: 1) the control is governed by an underlying stochastic process (occupant-location chain) and 2) sampled data is used. In general, the stability analysis of MJLS models is sophisticated, entailing verification of a set of linear matrix inequalities [22]. Here, we exploit the diffusive structure of the thermal dynamics at the sample times to verify moment boundedness when a low-gain PID control is used. We thus demonstrate that the expected squared deviation of the temperature at the occupant's current location from the goal temperature $E((y(t)-y_{\text{ref}})^2)$ remains bounded over time. The stability result is developed via an eigenanalysis of the recursion matrices H_1^{PID} and H_2^{PID}, which draws on properties of nonnegative matrices [31], [32] and eigenvalue sensitivity notions [33]. The result is formalized in the following theorem:

Theorem 1: Consider the closed-loop heat-flow dynamics in the case that the rooms are thermally connected, and the occupant-location Markov chain is ergodic. Assume that a PID control is used. For all sufficiently small negative feedback gains ($0 \leq K_p \leq \bar{K}_p$, $0 \leq K_d \leq \bar{K}_d$, and $0 \leq K_i \leq \bar{K}_i$, for some $\bar{K}_p > 0$, $\bar{K}_d > 0$, and $\bar{K}_i > 0$), the first- and second-moment vectors $\psi_1[k]$ and $\psi_2[k]$ are bounded for all k. Furthermore, the expected squared deviation $E((y(t)-y_{\text{ref}})^2)$ is bounded for all $t \geq 0$.

The proof of Theorem 1 can be found in Appendix IV. Theorem 1 demonstrates that low gain PID controllers achieve first- and second-moment boundedness and, hence, provides a baseline verification that occupant-location-catered controls can be developed for building HVAC systems.

Remark 4: The proof of Theorem 1 can be extended to obtain bounds on the gain parameters guaranteeing stability. However, bounds obtained in this way are typically conservative. Alternately, insight into the domain of stabilizing gains can be obtained by recognizing that stability is primarily modulated by three factors: 1) intrinsic bandwidth limits placed by the transfer functions from the HVAC input to each room's temperature (which depend on the thermal dynamics); 2) the

sampling period T; and 3) the transition rate of the Markov chain describing the occupant's location. Because of these factors, the gains that achieve stability are upper bounded. Specifically, the largest allowed gains are decided by the worst stability margin among transfer functions from the input to the possible occupant locations, provided that the transition rate of the occupant Markov chain is sufficiently slow compared to the time constants of the thermal process, and the sampling rate is sufficiently fast. However, a fast-switching occupant or slow sampling rate causes degradation in the allowed gains.

D. Performance Analysis and Tuning

Building thermal control is primarily concerned with maintaining adequate temperature regularity at a manageable actuation cost, in the face of disturbances. While low-gain controls maintain moment boundedness when the occupant-location-based control is used, larger gains or bandwidth may be required to adequately attenuate disturbances and track the reference. There is a need to understand whether occupant-location-catered controls can adequately regulate temperature with moderate actuation effort. In tandem, techniques are needed for tuning the PID controller's gains to meet regularity and actuation requirements. Thus, we consider tuning the control gains to optimize a quadratic performance metric which abstractly captures: 1) temperature regularity and 2) the effort expended for control. Specifically, the performance-tuning method optimizes a relative temperature-regularity plus actuation-effort metric. Specifically, the following quadratic metric is considered: $J = (1/T_2 - T_1)\sum_{k=T_1}^{T_2-1}(\alpha_1 z[k]^2 + \alpha_2 u[k]^2)$, where $z[k] = y_{\text{ref}} - y[k]$ is the temperature deviation of the occupied room from the reference, and $u[k]$ is the HVAC control input (volume flow rate from the HVAC system into the rooms). $[T_1, T_2]$ is the time interval of interest, and α_1 and α_2 are weighting factors. We note that energy required for the HVAC's air flow should roughly scale with $u[k]^2$, which suggests that a quadratic metric may be reasonable for energy expenditure in some settings. Likewise, a quadratic metric is used for the temperature regularity error.

Our primary interest is to characterize time-averaged metric J over a long horizon $[T_1, T_2]$. If the closed loop is two-moment-bounded, the underlying Markov chain is ergodic, and the disturbances are stationary, it can be shown that the time-averaged cost metric J approaches the steady-state ensemble average of the squared deviation cost in a probability-1 sense. Thus, the closed-loop performance can be computed as $\tilde{J} = \lim_{k\to\infty} E[\alpha_1 z[k]^2 + \alpha_2 u[k]^2]$, which can be expressed as: $\tilde{J} = \lim_{k\to\infty} \sum_{i=1}^{r} E[\alpha_1 z[k]^2 + \alpha_2 u[k]^2 \,|\, s[k] = i] Pr(s[k] = i)$. The summands in the expression for $\tilde{J}$ can be computed from entries in the first and second moments of the extended state vector, evaluated in steady state. In particular, the steady-state moments can be computed as the fixed point of (8), provided that the eigenvalues of H_1^{PID} and H_2^{PID} are strictly inside the unit circle and the disturbances are first- and second-moment stationaries. This fixed point is $\tilde{\Psi} = (I - H^{\text{PID}})^{-1}\tilde{D}$ where I is an identity matrix of appropriate size. The metric can then be computed as

$$\tilde{J} = \sum_{i=1}^{r} \alpha_1 F_1(i) + \alpha_2 F_2(i) \tag{7}$$

where $F_1(i) = \Psi_{lr+\bar{i}+(i-1)\tilde{A}-l+i}$ and $F_2(i) = (K_p + (K_d/T) + K_i T)^2 \Psi_{lr+\bar{i}+(i-1)\tilde{A}-l+i} + ((K_d/T))^2 \Psi_{lr+\bar{i}+(n+i-1)\tilde{A}-l+n+i} + (K_i T)^2 \Psi_{lr+ml^2} + (-2(K_d/T))(K_p + (K_d/T) + K_i T)\Psi_{lr+\bar{i}+(i-1)\tilde{A}-l+n+i} + (2TK_i)(K_p + (K_d/T) + K_i T)\Psi_{lr+\bar{i}+il} + (-2\ K_d K_i)\Psi_{lr+\bar{i}+(n+i)\tilde{A}-l}$, and where $\bar{i} = (i-1)\tilde{A} - l^2$.

The above explicit analysis of the expected metric allows evaluation, comparison, and tuning of the PID control, as illustrated in Section IV.

Remark 5: The proposed quadratic metric only aims to compare the relative performance of different control schemes with regard to temperature regularity and actuation effort, in an approximate sense. It does not aim to represent the full operating cost of the HVAC system, which may include fixed costs and operation-specific cost scalings. Likewise, an occupant's thermal comfort is decided by factors other than temperature, including personal choices and additional unmodeled environmental variables (e.g., humidity, air flow) [34], and hence, the metric also does not capture occupant comfort fully. Although the quadratic cost function is a significant abstraction of reality, it captures relevant tradeoffs in building thermal control and can provide an initial design which can be further tuned through simulation. If desired, similar analyses can be conducted for higher degree-polynomial metrics, using higher moment analyses of the MJLS.

IV. Example

The occupant-location-catered HVAC control scheme is evaluated in an example. A building with five thermally connected rooms, with topology shown in Fig. 1, is considered. The following parameters are assumed: the capacitances m_i are 8.94 e^{+4} J/K for the air in each room and 1.08 e^{+6} J/K for each wall, the thermal resistance of each wall face is $R_w = 5.71\ e^{-2}$ K/W, the convection resistance between each indoor room's air and a wall face is $R_{ci} = 6.67\ e^{-3}$ K/W the convection resistance between the outdoor air and each wall face is $R_{co} = 1.33\ e^{-2}$ K/W. The conductances w_{ij} between different nodes are inverses of these thermal resistances. The sampling interval is $T = 1$ second, and the occupant's location Markov chain has parameters $P_{ii} = 0.99975$ for $i = 1, \ldots, 5$, $P_{ij} = 6.25\ e^{-5}$ for $i \neq j$. The reference signal (desired temperature) is $y_{\text{ref}} = 21$ °C, and the initial temperatures are $x_i[0] = 25$ °C for $i = 1, \ldots, 15$. The system injects a larger air volume to the central room 4 as compared to the other rooms (specifically, $\gamma_4 = 0.5$ and $\gamma_i = (1/8)$ for $i = 1, 2, 3, 5$). The HVAC cold air temperature is 12 °C and it has a maximum capacity to inject 1 m^3/s cold air into the building. The following disturbances are modeled. The unmeasured heat gain in each room is modeled as a stationary process with mean 1 W and variance 1 in each room. The outside temperature is assumed to be sinusoid with a 24-h period, with a mean of 35°C and a peak of 42°C. Solar radiation is modeled as a rectified sine wave with a 24 h period,

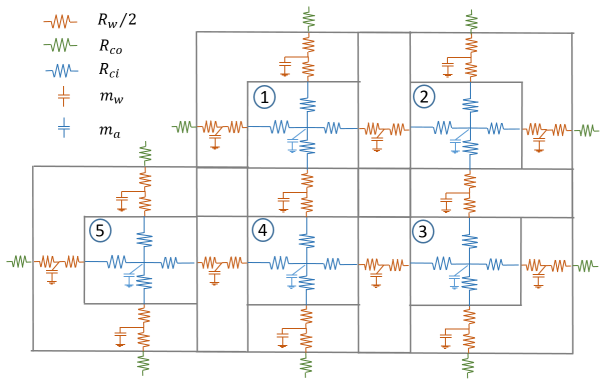

Fig. 1. Building diagram for the heat-flow model.

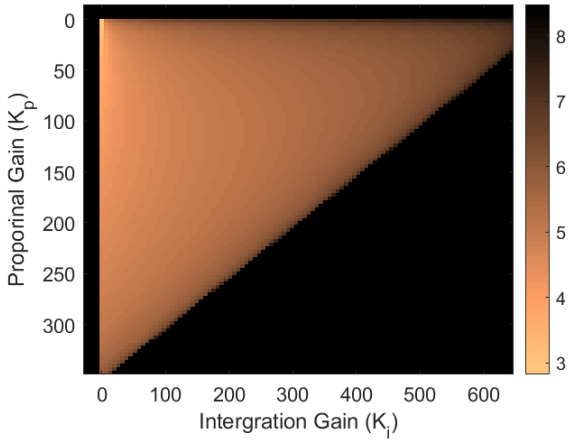

Fig. 2. Stability region and metric versus K_p and K_i. The dark-shaded areas correspond to unbounded moments, while the lighter shades show the metric on a logarithmic scale.

with an amplitude of 2 ($\mathrm{Wm}^2/$). The thermal parameters of the model are chosen to be similar to those used in other studies of building heat control systems, with the thermal capacitances and conductances (resistances) derived from typical material properties [14], [35]. The Markov chain for the occupant's location is chosen so that the occupant switches rooms on roughly an hourly basis, on average.

The following analyses were undertaken. Moment boundedness was determined as a function of the PID control gains, and the steady-state performance (cost) metric $E[\tilde{J}]$ was also evaluated. The gains were then tuned to optimize the performance metric. For the performance analysis, the cost function weightings were chosen as $\alpha_1 = 5$ and $\alpha_2 = 1$. Note that the performance analysis requires stationarity of the disturbances, and we approximated the periodic disturbances (outside temperature, solar radiation) as stationary processes with mean and variance computed from one period of the signal, for the purpose of gain tuning. However, the periodic disturbances were exactly simulated in testing the design.

For this example, the derivative term in the optimal PID controller was found to be unimportant, in the sense it introduced a filter of high bandwidth which had a negligible effect on the closed-loop dynamics. For this reason, the analysis and gain tuning were repeated for a PI-only control. Sufficiency of PI-only control is understandable since regulation and disturbance rejection are primary needs for the control. However, our methodology allows for the inclusion of a derivative controller, as needed. In the following, we present results for the PI controller analysis and design.

Fig. 2 shows the performance metric and stability (moment-boundedness) region as a function of K_p and K_i. Unstable gains are indicated with a dark color, while the metric is shown on a logarithmic scale in the stable region. As expected, moment boundedness is achieved for gains below a threshold. Fig. 3(a) shows simulations of the room temperatures for the optimally tuned control. The controller is able to regulate the temperature of the occupied room near the desired reference temperature, even as the temperatures in the other rooms deviate significantly from the reference. For example, room 4 is often overcooled because of the large volume flow into the room (we note that the deviations in nonoccupied rooms are somewhat exaggerated in this example because of the unequal volume flows). The input signal,

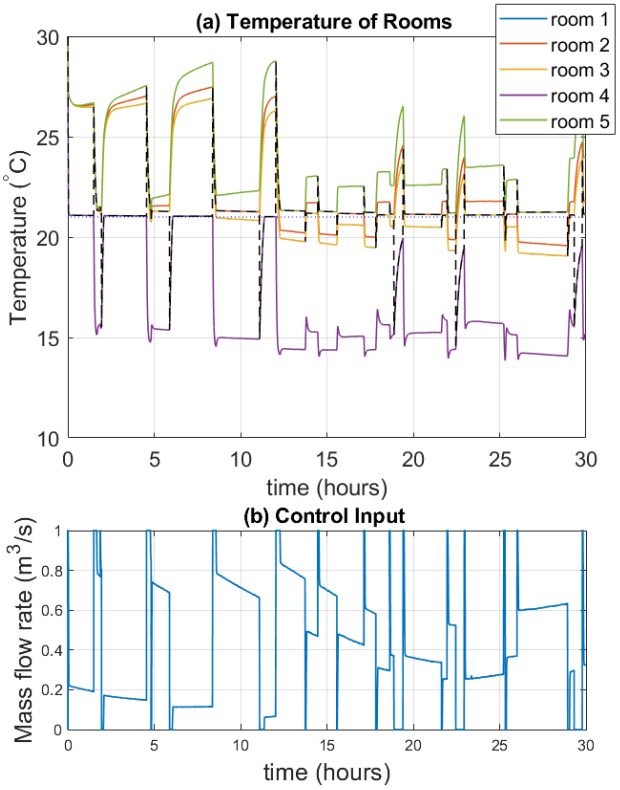

Fig. 3. Sample temperature dynamics for the optimal design ($K_p = 2.44$ and $K_i = 2.86e^{-6}$ for $(\alpha_1/\alpha_2) = 5$). (a) Temperature of rooms: dashed line indicates the occupied room. (b) Control input of system for optimal gains. (Total mass flow into the building.)

shown in Fig. 3(b), demonstrates that a persistent input is provided to maintain the desired temperature, with a larger input applied when the occupant changes rooms; the response time when the occupant switches rooms is primarily governed by the bandwidth of the building thermal dynamics. The simulations suggest that the occupant-location-catered scheme is able to adequately regulate the temperature at the occupant's location.

The dependence of the stability region on model parameters was also studied, by determining the maximum stabilizing proportional gain K_p upon scaling up of the optimal design. We determined the dependence of this maximum gain on: 1) the room-transition probability; 2) the sampling time T; and 3) the volume air flow fractions. For this example, the maximum allowed gain was found to be unchanging over a wide set of transition probabilities and sampling times. This insensitivity is understandable since the nominal sampling time is short, and the room-transition times are long compared to the building thermal processes. To study the dependence of the stability region on the volume air flow fractions, the percentage of the volume air flow to the central room (Room 4) is changed and the other percentages were correspondingly altered. For the baseline, the maximum allowed gain (with the ratio of K_p to K_i fixed at the optimal) was $K_p = 354.75$. If the air flow is distributed equally to all rooms, the maximum allowed gain increases to $K_p = 886.25$. On the other hand, if the air flow ratio fraction to the central room increases to 75%, the maximum allowed gain decreases to $K_p = 236.5$. Thus, we see that the stability region grows with more equally distributed volume air flow.

The dependence of the gain tuning on the cost-function parameters α_1 and α_2 was determined. We found that the optimal tuning required larger integral gains, when α_1 was increased. Specifically, for (α_1/α_2) =1,5, 10, 50, and 100, the optimal integral gains were found to be $K_i = 2.23e^{-8}$, 2.68 e^{-6}, 1.6 e^{-3}, 5.3 e^{-3}, and 8 e^{-3}, respectively. This increase in the integral gain matches the intuition that increasing α_1 would prefer accurate regulation rather than low input cost.

Finally, the optimal occupant-location-catered design has been compared with an optimal fixed PI control scheme, where a thermostat in Room number 4 is used for control. The actuation effort and temperature regularity metric values for the occupant-location-catered scheme are 374.97 and 41.49, and are $1.08e^{+4}$ and $1.64e^{+3}$ for the fixed scheme. Thus, the catered scheme is found to significantly improve regularity, with modification in actuation effort simultaneously.

V. Conclusion

Thermal regularization strategies for buildings that cater to the changing location of an occupant have been studied. Stochastic stability of the closed-loop dynamics was verified using an MJLS formulation of the model. Also, controller parameter tuning to optimize a quadratic cost function, which encompasses regularization and control-effort terms, was considered. The control strategy was applied to a case study, which demonstrated that the occupant-location-catered approaches may have considerable performance benefits compared to the traditional fixed-thermostat-based controls.

Appendix
Proof of Theorem 1

Proof: First, we show that given bounded disturbances the eigenvalues of H_1^{PID} and H_2^{PID} decide boundedness of the extended state vector's moments. Consider

$$\tilde{\psi}[k] = \begin{bmatrix} \psi_1[k] \\ \psi_2[k] \end{bmatrix}.$$

We can show the first and second moments of $\tilde{\psi}[k]$ are bounded if all eigenvalues H_1^{PID} and H_2^{PID} are inside the unit circle. For that, let us combine the first- and second-moment recursions as

$$E(\tilde{\psi}[k+1]) = H^{\text{PID}} E(\tilde{\psi}[k]) + \tilde{D}[k] \tag{8}$$

where

$$H^{\text{PID}} = \begin{bmatrix} H_1^{\text{PID}} & \bar{O} \\ H_{12}^{\text{PID}} & H_2^{\text{PID}} \end{bmatrix}, \tilde{D}[k] = \begin{bmatrix} \tilde{D}_1[k] \\ \tilde{D}_2[k] \end{bmatrix}$$

and $\bar{O}$ is zero matrix of appropriate dimension. Equation ((8)) specifies a linear time-invariant dynamics. Further, since $E(\bar{D}[k])$ and $E(\bar{D}[k]^{\otimes 2})$ are bounded, it also follows that $\tilde{D}_1[k]$ and $\tilde{D}_2[k]$ are bounded. Thus, $E(\tilde{\psi}[k])$ is bounded provided that all eigenvalues H^{PID} are inside the unit circle, or equivalently the eigenvalues H_1^{PID} and H_2^{PID} are inside the unit circle.

Next, we need to show that all eigenvalues of H_1^{PID} and H_2^{PID} are strictly inside the unit circle for sufficiently small K_p, K_d, and K_i. The eigenanalysis is achieved according to the following five steps.

Step 1: Several properties of the matrices $G_c^{\text{PID}}(i)$ are determined. The principal submatrix of $G_c^{\text{PID}}(i)$ consisting of the first n rows and columns is considered. We call this matrix $G_c^P(i)$. We note $G_c^P(i) = \bar{A} - K_p \bar{\Phi}_{\bar{\beta}} S_2(i) - (K_d/T)\bar{\Phi}_{\bar{\beta}} S_2(i) - K_i T \bar{\Phi}_{\bar{\beta}} S_2(i)$, where $\bar{\Phi}_{\bar{\beta}}$ is the principal submatrix of $\Phi_{\bar{\beta}}$ made up of its first n rows and columns, and $\bar{A} = e^{-TA}$. The matrix A is an (asymmetric) grounded Laplacian matrix or nonsingular M-matrix. Furthermore, from the assumption that all rooms are thermally connected, the digraph associated with A has a directed spanning tree with vertex n as the root. It is immediate that eigenvalues of A are strictly in the open right half-plane. Since A is a nonsingular irreducible M-matrix, $\bar{Q} = e^{-AT}$ is strictly positive [31], [32]. Also, note that $K_p \bar{\Phi}_{\bar{\beta}} S_2(i)$, $(K_d/T)\bar{\Phi}_{\bar{\beta}} S_2(i)$, and $K_i T \bar{\Phi}_{\bar{\beta}} S_2(i)$ have strictly negative entries in the ith column, and are zero otherwise. Furthermore, for any sufficiently small K_p, K_d, and K_i (less than some $\bar{K}_p$,$\bar{K}_d$, and $\bar{K}_i$), the entries in the ith column of $-K_p \bar{\Phi}_{\bar{\beta}} S_2(i) - (K_d/T)\bar{\Phi}_{\bar{\beta}} S_2(i) - K_i T \bar{\Phi}_{\bar{\beta}} S_2(i)$ are strictly less than the entries in the ith column of $\bar{A}$ in magnitude. Thus, it follows immediately that $G_c^P(i)$ is strictly positive with row sums strictly less than 1.

Step 2: Now consider another principal submatrix of G_c^{PID} consisting of its first $n+r$ rows and columns, which we call G_c^{PD}. The matrix can be written as

$$\begin{bmatrix} G_c^{PD} & \dfrac{K_d}{T}\bar{\Phi}_{\bar{\beta}} S_2(i) \\ I_{r\times n} & 0_{r\times r} \end{bmatrix}.$$

We argue that the eigenvalues of the substochastic matrix G_c^{PD} are strictly inside the unit circle. To do so, we note that the first n rows of the matrices have row sums strictly less than 1. Considering the graph associated with this substochastic

matrix, we see immediately that there is a path from every vertex to a vertex whose outdegree (corresponding matrix row sum) is strictly less than 1. It thus follows that the eigenvalues of the matrix are strictly within the unit circle.

Step 3: The closed-loop MJLS state matrix when the PID controller is used can be expressed in terms of G_c^{PD}, as follows:

$$G_c^{\text{PID}}(i) = \begin{bmatrix} G_c^{PD}(i) & \bar{\epsilon}(i) \\ \vec{V}(i) & 1 \end{bmatrix}.$$

Here, $\bar{\epsilon}(i)$ is column vector with $n+r$ entries which all equal zero except the ith entry, which is equal to $-\epsilon$, where $\epsilon = K_i T$. Also, $\vec{V}(i)$ is the row vector with $n+r$ entries, whose ith entry is equal to 1 and remaining entries are zero.

Step 4: Substituting the above form of the matrix $G_c^{\text{PID}}(i)$ into H_1^{PID}, we have

$$H_1^{\text{PID}} = \begin{bmatrix} p_{11}\begin{bmatrix} \bar{G}_c^{PD}(1) & \bar{\epsilon}(1) \\ \vec{V}(1) & 1 \end{bmatrix} & \cdots & p_{1b}\begin{bmatrix} \bar{G}_c^{PD}(n) & \bar{\epsilon}(n) \\ \vec{V}(n) & 1 \end{bmatrix} \\ \vdots & \ddots & \vdots \\ p_{b1}\begin{bmatrix} \bar{G}_c^{PD}(1) & \bar{\epsilon}(1) \\ \vec{V}(1) & 1 \end{bmatrix} & \cdots & p_{bb}\begin{bmatrix} \bar{G}_c^{PD}(n) & \bar{\epsilon}(n) \\ \vec{V}(n) & 1 \end{bmatrix} \end{bmatrix}. \quad (9)$$

By permuting H_1^{PID} appropriately, we can simplify the eigenanalysis of the matrix. Specifically, the matrix $\tilde{H}_1^{\text{PID}}$ is defined as a permutation of H_1^{PID}, where the rows lz_1, $z_1 = 1, \ldots, r$, are placed at the bottom of the matrix and likewise the columns lz_2, $z_2 = 1, \ldots, r$ are placed at the right of the matrix (in order). The permuted matrix is given by

$$\tilde{H}_1^{\text{PID}} = \begin{bmatrix} F_1 & \tilde{\epsilon} \\ \tilde{V} & P \end{bmatrix} \quad (10)$$

where

$$F_1 = \begin{bmatrix} p_{11}\bar{G}_c^{PD}(1) & \cdots & p_{1n}\bar{G}_c^{PD}(n) \\ \vdots & \ddots & \vdots \\ p_{n1}\bar{G}_c^{PD}(1) & \cdots & p_{nn}\bar{G}_c^{PD}(n) \end{bmatrix}$$

$$\text{and } \tilde{\epsilon} = \begin{bmatrix} p_{11}\bar{\epsilon}(1) & \cdots & p_{1n}\bar{\epsilon}(n) \\ \vdots & \ddots & \vdots \\ p_{n1}\bar{\epsilon}(1) & \cdots & p_{nn}\bar{\epsilon}(n) \end{bmatrix}$$

$$\text{and } \tilde{V} = \begin{bmatrix} p_{11}\vec{V}(1) & \cdots & p_{1n}\vec{V}(n) \\ \vdots & \ddots & \vdots \\ p_{n1}\vec{V}(1) & \cdots & p_{nn}\vec{V}(n) \end{bmatrix}.$$

If ϵ is equal to zero (i.e., no integral term is used), then $\tilde{H}_1^{\text{PID}}$ has lower triangular structure and its eigenvalues are equal to the union of the eigenvalues of F_1 and P. It is easy to show all eigenvalues of F_1 are inside the unit circle using the same graphical argument used in step 2 for the eigenvalues G_c^{PD}. Also, P has one eigenvalue equal to one, while the remaining eigenvalues are strictly inside the unit circle. Now, from the eigenvalue perturbation theory, the eigenvalues of $\tilde{H}_1^{\text{PID}}$ can be contained in circles in the complex plane around the eigenvalues prior to perturbation, whose radii approach 0 as ϵ. Thus, by scaling down K_i, all eigenvalues except the eigenvalue at 1 necessarily remain within the unit circle. It remains to show that the eigenvalue of $\tilde{H}_1^{\text{PID}}$ which equals 1 for $\epsilon = 0$, moves into the unit circle for sufficiently small positive ϵ. This can be shown using an eigenvalue sensitivity analysis. Using the fact that the matrix $\tilde{H}_1^{\text{PID}}$ is nonnegative for $\epsilon = 0$, both left and right eigenvectors associated with the unity eigenvalue are seen to be nonnegative. Indeed, it can be seen from the reducibility structure of $\tilde{H}_1^{\text{PID}}$ that the final r entries of the right eigenvector are strictly positive, while all entries of the left eigenvector are strictly positive. Also, $\tilde{\epsilon}$ is nonpositive for nonzero ϵ. Therefore, from the eigenvalue sensitivity formula, the first-order sensitivity of the eigenvalue is seen to be strictly negative. It thus follows that all eigenvalues of $\tilde{H}_1^{\text{PID}}$ and H_1^{PID} are strictly within the unit circle for sufficiently small K_i.

Step 5: An entirely analogous argument can be used to prove that eigenvalues of H_2^{PID} are strictly within the unit circle for small control gains. These properties follow immediately from an expansion of the Kronecker product, whereupon the analogous logic as steps 1–4 can be used to characterize the spectrum. According to the discussion at the beginning of the proof, since the eigenvalues of H_1^{PID} and H_2^{PID} are within the unit circle, $\psi_1[k]$ and $\psi_2[k]$ are bounded. Since the first and second moments of $x[k]$ are linear functions of $\psi_1[k]$ and $\psi_2[k]$, the moments of $x[k]$ are also verified to be bounded. It remains to show that the expected squared deviation $E((y(t) - y_{\text{ref}})^2)$ is bounded for all $t \geq 0$. This can be evident when $y(t) - y_{\text{ref}}$ is a linear function of $x[k^*]$, where k^* is greatest integer less than $\frac{t}{T}$. Since $y(t) - y_{\text{ref}}$ is computed from $x[k^*]$ by solving the closed-loop system over the interval $[k^*T, t]$, where $t < (k^*+1)T$, it follows that the linear mapping between $x[k^*]$ and $y(t) - y_{\text{ref}}$ is uniformly bounded. Thus, it follows that the expected squared deviation $E((y(t) - y_{\text{ref}})^2)$ is a linear function of $\psi_1[k]$ and $\psi_2[k]$ which is uniformly bounded. Hence, the expected squared deviation is bounded. □

REFERENCES

[1] J. Gubbi, R. Buyya, S. Marusic, and M. Palaniswami, "Internet of Things (IoT): A vision, architectural elements, and future directions," *Future Gener. Comput. Syst.*, vol. 29, no. 7, pp. 1645–1660, Sep. 2013.

[2] C. Wei and Y. Li, "Design of energy consumption monitoring and energy-saving management system of intelligent building based on the Internet of Things," in *Proc. IEEE Int. Conf. Electron., Commun. Control (ICECC)*, Ningbo, China, Sep. 2011, pp. 3650–3652.

[3] L. Mainetti, L. Patrono, and A. Vilei, "Evolution of wireless sensor networks towards the Internet of Things: A survey," in *Proc. IEEE 19th Int. Conf. Softw., Telecommun. Comput. Netw. (SoftCOM)*, Split, Croatia, Sep. 2011, pp. 1–6.

[4] N. K. Suryadevara and S. C. Mukhopadhyay, "Wireless sensor network based home monitoring system for wellness determination of elderly," *IEEE Sensors J.*, vol. 12, no. 6, pp. 1965–1972, Jun. 2012.

[5] K. Doty, S. Roy, and T. R. Fischer, "Explicit state-estimation error calculations for flag hidden Markov models," *IEEE Trans. Signal Process.*, vol. 64, no. 17, pp. 4444–4454, Sep. 2016.

[6] Z. Qin, G. Denker, C. Giannelli, P. Bellavista, and N. Venkatasubramanian, "A software defined networking architecture for the Internet-of-Things," in *Proc. IEEE Netw. Oper. Manage. Symp. (NOMS)*, Kraków, Poland, May 2014, pp. 1–9.

[7] S. Roy *et al.*, "Client-catered control of engineered spaces with software-defined sensors and actuators," in *Proc. IEEE Int. Conf. Smart Comput. (SMARTCOMP)*, St. Louis, MO, USA, May 2016, pp. 1–8.

[8] A. F. Robertson and D. Gross, "An electrical-analog method for transient heat-flow analysis," *J. Res. Nat. Bur. Standards*, vol. 61, no. 2, pp. 105–115, Aug. 1958.

[9] K. Deng, P. Barooah, P. G. Mehta, and S. P. Meyn, "Building thermal model reduction via aggregation of states," in *Proc. IEEE Amer. Control Conf. (ACC)*, Baltimore, MD, USA, Jun./Jul. 2010, pp. 5118–5123.

[10] A. Parisio, M. Molinari, D. Varagnolo, and K. H. Johansson, "A scenario-based predictive control approach to building HVAC management systems," in *Proc. IEEE Int. Conf. Autom. Sci. Eng. (CASE)*, Madison, WI, USA, Aug. 2013, pp. 428–435.

[11] A. Parisio, D. Varagnolo, D. Risberg, G. Pattarello, M. Molinari, and K. H. Johansson, "Randomized model predictive control for HVAC systems," in *Proc. 5th ACM Workshop Embedded Syst. Energy-Efficient Buildings*. Roma, Italy, Nov. 2013, pp. 1–8.

[12] B. Lim, M. van den Briel, S. Thiebaux, S. Backhaus, and R. Bent, "HVAC-aware occupancy scheduling," in *Proc. AAAI*, Austin, TX, USA, Jan. 2015, pp. 4249–4250.

[13] N. Skeledzija, J. Cesic, E. Koco, V. Bachler, H. N. Vucemilo, and H. Dzapo, "Smart home automation system for energy efficient housing," in *Proc. IEEE 37th Int. Conv. Inf. Commun. Technol., Electron. Microelectron. (MIPRO)*, Opatija, Croatia, May 2014, pp. 166–171.

[14] M. M. Haghighi, "Modeling and optimal control algorithm design for HVAC systems in energy efficient buildings," EECS Dept., Univ. California, Berkeley, CA, USA, Tech. Rep. UCB/EECS-2011-12, Feb. 2011.

[15] M. Maasoumy, A. Pinto, and A. Sangiovanni-Vincentelli, "Model-based hierarchical optimal control design for HVAC systems," in *Proc. ASME Dyn. Syst. Control Conf. Bath/ASME Symp. Fluid Power Motion Control*, 2011, pp. 271–278.

[16] S. Goyal, C. Liao, and P. Barooah, "Identification of multi-zone building thermal interaction model from data," in *Proc. 50th IEEE Conf. Decis. Control Eur. Control Conf. (CDC-ECC)*, Dec. 2011, pp. 181–186.

[17] S. Katipamula and M. R. Brambley, "*Review article*: Methods for fault detection, diagnostics, and prognostics for building systems—A review, part I," *HVAC R Res.*, vol. 11, no. 1, pp. 3–25, 2005.

[18] A. R. Al-Ali, I. A. Zualkernan, M. Rashid, R. Gupta, and M. Alikarar, "A smart home energy management system using IoT and big data analytics approach," *IEEE Trans. Consum. Electron.*, vol. 63, no. 4, pp. 426–434, Nov. 2017.

[19] B. Dong, K. P. Lam, and C. Neuman, "Integrated building control based on occupant behavior pattern detection and local weather forecasting," in *Proc. 12th Int. IBPSA Conference.*, Sydney, NSW, Australia, Nov. 2011, pp. 14–17.

[20] S. Goyal, H. A. Ingley, and P. Barooah, "Occupancy-based zone-climate control for energy-efficient buildings: Complexity vs. performance," *Appl. Energy*, vol. 106, pp. 209–221, Jun. 2013.

[21] J. Shi, N. Yu, and W. Yao, "Energy efficient building HVAC control algorithm with real-time occupancy prediction," *Energy Procedia*, vol. 111, pp. 267–276, Mar. 2017.

[22] X. Feng, K. A. Loparo, Y. Ji, and H. J. Chizeck, "Stochastic stability properties of jump linear systems," *IEEE Trans. Autom. Control*, vol. 37, no. 1, pp. 38–53, Jan. 1992.

[23] O. L. V. Costa, M. D. Fragoso, and R. P. Marques, *Discrete-Time Markov Jump Linear Systems*. New York, NY, USA: Springer, 2006.

[24] D. P. D. Farias, J. C. Geromel, J. B. R. D. Val, and O. L. V. Costa, "Output feedback control of Markov jump linear systems in continuous-time," *IEEE Trans. Autom. Control*, vol. 45, no. 5, pp. 944–949, May 2000.

[25] S. Roy and A. Saberi, "Static decentralized control of a single-integrator network with Markovian sensing topology," *Automatica*, vol. 41, no. 11, pp. 1867–1877, Nov. 2005.

[26] S. Roy, G. C. Verghese, and B. C. Lesieutre, "Moment-linear stochastic systems," in *Proc. Inform. Control, Autom. Robot. I*, 2006, pp. 263–271.

[27] A. Vosughi and S. Roy, "Occupant-location-catered control of IoT-enabled building HVAC systems," in *Proc. 5th IEEE Global Conf. Signal Inf. Process.*, Montreal, QC, Canada, Nov. 2017, pp. 813–817.

[28] S. Roy and R. Dhal, "Situational awareness for dynamical network processes using incidental measurements," *IEEE J. Sel. Topics Signal Process.*, vol. 9, no. 2, pp. 304–316, Mar. 2015.

[29] V. S. K. V. Harish and A. Kumar, "A review on modeling and simulation of building energy systems," *Renew. Sustain. Energy Rev.*, vol. 56, pp. 1272–1292, Apr. 2016.

[30] N. Aschenbruck, A. Munjal, and T. Camp, "Trace-based mobility modeling for multi-hop wireless networks," *Comput. Commun.*, vol. 34, no. 6, pp. 704–714, 2011.

[31] P. Santesso and M. E. Valcher, "On the zero pattern properties and asymptotic behavior of continuous-time positive system trajectories," *Linear Algebra Appl.*, vol. 425, nos. 2–3, pp. 283–302, Sep. 2007.

[32] A. Berman and R. J. Plemmons, *Nonnegative Matrices in the Mathematical Sciences* (SIAM Classics in Applied Mathematics). Philadelphia, PA, USA: SIAM, 1994.

[33] J. H. Wilkinson, *The Algebraic Eigenvalue Problem*, vol. 87. Oxford, U.K.: Clarendon Press, 1965.

[34] L. Fang, G. Clausen, and P. O. Fanger, "Impact of temperature and humidity on the perception of indoor air quality," *Indoor Air*, vol. 8, no. 2, pp. 80–90, 1998.

[35] M. B. Wilson, R. Luck, and P. J. Mago, "A first-order study of reduced energy consumption via increased thermal capacitance with thermal storage management in a micro-building," *Energies*, vol. 8, no. 10, pp. 12266–12282, Oct. 2015.